Perfluorinated Coatings and Terracotta: an Impregnation Study

Ali Youssef,[1] Martial Pabon,[2] Emmanuel Woelflé,[2] Romain Severac,[2] Robert G. Gilbert[1]

[1]*CNAFS/Land Crop & Food Sciences, The University of Queensland, Brisbane, Queensland 4072, Australia*
[2]*Du Pont de Nemours, F - 78711 Mantes-La-Ville, BP 1025 - 78202 Mantes-La-Jolie Cedex, Paris, France*

Received 25 April 2007; accepted 12 May 2008
DOI 10.1002/app.28702
Published online 9 July 2008 in Wiley InterScience (www.interscience.wiley.com).

ABSTRACT: The mechanisms of penetration onto terracotta of two commercially available perfluorinated acrylates were studied: Zonyl®225, a solvent-based perfluorinated polyacrylate containing two unfluorinated acrylic or vinylic monomers; and Zonyl®329, an aqueous dispersion synthesized from comparable monomers plus a vinylic silane. Two application methods were used: by immersion of the substrate for 15 h and by multiple brush strokes, with pauses between strokes. Application effectiveness was assessed by measuring the depth of penetration into terracotta. The results of coating were examined by optical and electron microscopy, including elemental analysis. When the impregnating agent was applied by extended immersion, both solvent-based and aqueous dispersion exhibited higher penetration depths with increasing concentrations. When applied using multiple brush strokes, the solvent-based solution exhibited the same trend as that in immersion; however, the aqueous dispersion showed no penetration beyond $\sim$ 0.12 mm. This limited depth of penetration is shown to be a result of partial drying between brush strokes, but also as a result of porosity restrictions and electrostatic interactions between the positively charged polymer colloids in the dispersion and the negatively charged terracotta surface. © 2008 Wiley Periodicals, Inc. J Appl Polym Sci 110: 663–677, 2008

Key words: coatings; diffusion; electron microscopy; surfaces; fluoropolymers

INTRODUCTION

In both outdoor and indoor settings, porous materials are subjected to physical, biological, and chemical wear. The chemical corrosion experienced by porous materials outdoors comes as a result of exposure to water in the form of rain, snow, or moisture. Such exposure can lead to oxidation and hydration reactions, accompanied with dissolution and solubilization of elements and minerals.[1] Physical wear is also likely to occur, especially in outdoor settings such as driveways and patios. Porous materials in the household are also exposed to deterioration; this comes primarily in the form of high staining household products (anything from coffee to oil) being spilled onto porous masonry. Such materials are easily absorbed via capillarity and in most cases are impossible to remove.

Today's urban environment has led to a rapid rise in the rate of deterioration of porous building materials. This is primarily because of the increase in atmospheric pollution which has lead to a rise in the concentration of organic and inorganic compounds in the microenvironment of the porous material.[2] Atmospheric pollutants lead to a darkening and staining of stone surfaces, reducing the esthetic appeal of a substrate. Such pollutants over a prolonged period also lead to structural deterioration of porous substrates.[3–8] Pollution effects are compounded by areas of high abrasion, mainly in the form of floor tiles around the house or work environment. In most cases such surfaces need to be protected against both oil and water along with being able to tolerate a certain amount of abrasion while still being able to offer the repellencies required.

In the case of baked clays such as terracotta, the migration of soluble salts into the substrate leads to efflorescences as the saline solution moves through the pore network toward the surface.[9] Degradation of the terracotta then proceeds as the salts crystallize at the surface or below it.[10] Concurrently, organic particles responsible for the darkening or soiling of the surface are cemented by these recrystallized salts. Reducing the rate of decay of such materials therefore requires both hydrophobic and oleophobic treatment.[11]

Of the protective measures currently available, fluorine-based coatings are the most effective. Fluorinated polymers furnish materials with special properties, such as low refractive index and

Correspondence to: R. G. Gilbert (b.gilbert@uq.edu.au).
Contract grant sponsors: Australian Research Council, and of EI DuPont de Nemours Inc.

dielectric constants,[12] low surface energy,[13] high chemical and thermal stability,[14] and all-round weatherability.[15] Comb-shaped perfluorinated polymers, with close packed fluoroalkyl groups, can impart a surface energy of less than 10 mN m^{-1}, preventing the adhesion/absorption of contaminants.[16] Such properties of fluorinated polymers have seen them rise in importance with regards to the conservation of both ancient and modern buildings and monuments.

Ideally, stone protectants should exhibit not only water and oil repellency but also transparency, colorlessness, weatherability, and permeability to water vapor and gases.[17] Most of these polymer-based protectants take the form of dispersions of the polymer in a continuous medium, either as a solution in an organic solvent or as a polymer colloid of a hydrophobic polymer in water.[15,18,19] These coatings need to exhibit breathability (water-vapor transmission) and thus have repellency without complete blocking of pores, as happens when a paint forms an impermeable film.[20]

One of the most important factors in stone coating is that surface coatings should exhibit a high penetration depth and low solids content.[21] No coating is permanent, especially when exposed to the outdoors; consecutive applications are usually required, with the time between applications determined by the durability of the coating. Many key properties in stone care hinge on a deep penetration depth for the protective polymer. Porous surfaces will decay over time, especially in areas of high wear; as the decay progresses, new layers of the substrate surface are revealed. A deeper penetration will ensure protection regardless of the depth the deterioration has reached. Over a period of time this also reduces the cost of reapplication. Ascertaining what properties control depth of penetration, and the mechanisms of this process, will give an insight into the performance of the coating; deeper penetrating coatings will require fewer reapplications.

Penetration depth is controlled both by the chemical nature of the coating and of the substrate and any subsequent interactions, but should also be affected by the application method. Substrate properties such as porosity, affinity of binding to polymer, and chemical composition are usually beyond control, especially with natural stones. A porous material can take up water (or impregnating agent in this case) by coming into contact with the impregnating agent and without any external pressure. This occurs through capillarity and is affected by the size and shape of pores as well as the structure of the porous network.[22] Our study looks at how penetration depth is influenced by some controllable features of the coating process, particularly the mode of application and the chemical formulation.

A high density of polymer (per unit volume of substrate) with a small penetration depth suggests the coating is not efficient and is likely to alter the optical properties of the stone leading to skin formation. This is where the surface layer of the coating solidifies to form a skin, underneath which remains a liquid; this layer acts as a barrier to penetration. Higher penetration depths will mean that the coating density is reduced.

The aims of this work are to link application methods of coatings, their medium (solution or polymer colloid) and polymer properties to the depth of penetration. Understanding such fundamental relationships will allow for the creation of improved fluorinated coatings specifically devised and tailored to a particular substrate.

Here we report on the relationship between the method of applying an impregnating agent and the interactions involved in the coating process to the penetration depth into a substrate. This is achieved by testing two methods of application onto terracotta: brush and immersion. Measurements of the diffusion of each impregnating agent into the terracotta can be rationalized in terms of the substrate properties, the chemical formulation of the coating, and the application method. Two chemical formulations of fluorinated acrylates as used: cationic water dispersion (a polymer colloid) and a solvent-based solution.

MATERIALS AND METHODS

Terracotta characterization

Terracotta pavers of 13 mm thickness were used in all experiments; these were cut down to size accordingly. All terracotta was provided by Guiraud Frères, F-31250, Revel, France.

Capillary absorption

This was determined by using the gravimetric sorption technique, using the so-called "Normal" protocol.[23] Initially, the stone sample is dried at 110°C for 48 h under vacuum. The surface to be treated is then laid on a filter paper pad approximately 1 cm thick, which has been partially immersed in water at room temperature and pressure. By weighing specimens after 10, 20, and 30 min and 1, 2, 4, 8, 48, 72, and 96 h, the amount of water absorbed by capillary forces and thus the capillary absorption coefficient can be determined. This was done with solutions of both white spirits and Milli-Q water, as used to dilute the two coatings before being applied to a surface.

The amount of capillary absorption of a solvent is found using:

$$Q_{\text{cap}} = \frac{(M_i - M_0)}{S} \quad (1)$$

where Q_{cap} is the mass of absorbed solvent per unit surface area of the substrate, M_i is the sample mass at time t, M_0 is the dry sample mass, and S is the area of the substrate surface in contact with the partially immersed pad. The absorption coefficient A is obtained if capillary absorption follows a simple diffusion process, in which case:

$$Q_{\text{cap}} = At^{1/2} \quad (2)$$

Absorption by complete immersion

This method was carried out by gravimetry, using a modified version of the Normal protocol.[24] The stone sample, having previously been dried at 110°C for 48 h under vacuum, is completely immersed in either solvent/dispersant or polymer solution/dispersion, under constant stirring; this is especially important in the case of the dispersion, which will separate on standing. Terracotta tiles were immersed in the impregnating agent at 0, 0.5, 5.5, and 10.5% solids of both Zonyl®329 and Zonyl®225. All experiments were conducted at room temperature and pressure. Measurements were taken at 0, 10, 20, and 30 min and 1, 4, 6, 8, 24, 48, and 96 h.

The fraction of coating absorbed, Q_{imm}, at time t, is found from:

$$Q_{\text{imm}} = \frac{M_i - M_0}{M_0} \quad (3)$$

where M_i and M_0 are as defined earlier. A plot of Q_{imm} against t gives an absorption curve that shows the difference in uptake of both polymers.

Mercury porosimetry

Intrusion porosimetry, to obtain information on pore size, was implemented using a Micrometrics Autopore II (9220).

X-ray diffraction analysis

An elemental analysis of two terracotta cross-sections from the same piece was performed to see if the substrate/polymer interactions were uniform with depth. Two segments, surface and mid-section, were cut using a diamond saw and analyzed using a Shimadzu XRD-6000 (Kyoto, Japan), Ni-filtered Cu Kα radiation ($\lambda = 1.5406$ E), generator voltage of 40 kV and current of 30 mA. Samples were scanned at room temperature as solids and the scanning range was varied from $2\theta = 3^\circ - 70^\circ$, at a scanning rate of 1.2° min^{-1}.

Surface charge analysis

Pore surface charge was analyzed by crushing the terracotta in an impact mill and then sieving the sample to a particle size range between 150 and 200 μm. The milled terracotta was then analyzed using an Electro Kinetic Analyzer (EKA) from Anton Paar (Richmond, VA). Using a cylindrical cell, with a 25 μm PA filter, the electrolyte solution was made up using the same mono-acid used as a pH controller in Zonyl®329, and MQ-water at pH 4.6–4.7.

Zonyl® characterization

Molecular weights

A number average molecular weight ($\overline{M}_n$) range for Zonyl®329 and Zonyl®225 was measured using an Agilent 1100 series SEC (Santa Clara, CA), with Agilent Chem Station GPC data analysis software, columns 2 × PLgel 5μ MIXED-C + Guard column, run at 40°C, flow rate 1.00 mL min^{-1}, injection volume 100 μL, run time 23.5 min, equipped with a refractive index detector and poly(methyl methacrylate) standards for calibration. Zonyl®329 measurements were performed in acetone and trifluoroacetic acid at 10 g L^{-1}. Zonyl®225 was measured in tetrahydrofuran.

Photon correlation spectroscopy

The particle size distribution of the water dispersion was analyzed using a Brookhaven PCS BI-200SM Version 2 goniometer (Holtsville, NY) with 633 nm 35 mW HeNe laser equipped with a BI-APD Avalanche Photodiode Detector and PC1 B1-9000AT EN correlator at 25°C. Data were fitted using both the CONTIN and NLLS methods (see below). A refractive index of 1.45 was used for the aqueous dispersion.[25] Samples were made up between 0.06 and 0.1% solids (which is judged sufficiently dilute to avoid aggregation) and the count rate did not exceed 5 × 105 s^{-1}. It will be recalled that photon correlation spectroscopy (PCS) measures the z-average hydrodynamic radius.

Thermal analysis

The glass transition temperature(s), T_g, and the fluoropolymer isotropization (T_i) and crystallization (T_c) temperatures were determined for both Zonyl® products through differential scanning calorimeter measurements (TA Instruments DSC Q2000, New Castle, DE, cycled at 3°C min^{-1} from −60 to +100°C, and isothermal at +100°C for 5 min, $N_{2(g)}$ flow rate at 50 mL min^{-1}) on dry samples of mass 6–8 mg. To ensure samples were completely dry, solutions of

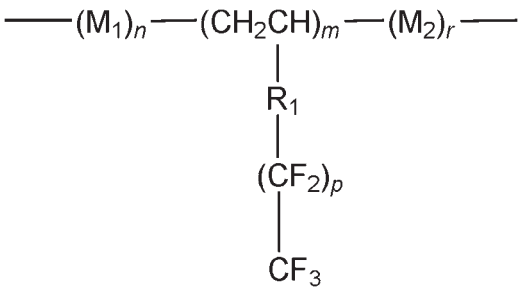

Figure 1 Formulae for Zonyl® coatings used; M_1 and M_2 are acrylic and/or vinylic comonomers, and R_1 is a ester group.

Zonyl® were dried at room temperature in Teflon pans for 48 h, before being placed at room temperature under vacuum for a further 48 h.

Surface tension

Surface tension measurements were conducted at concentrations of 0, 0.5, 5.5, and 10.5%, at 25°C, on a NIMA ST500 surface tensiometer (Coventry, UK), using the Wilhelmy plate method.

Zeta potential

Zeta potential and conductivity were determined using a Zetasizer Nano Series ZS from Malvern Instruments Ltd (Worcestershire, UK), with folded capillary cells and standard operating procedure.

Rheology

A Rheometrics Advanced Rheometric Expansion System (ARES) rheometer (Piscataway, NJ) was used to measure the viscosity of Zonyls® at room temperature. Undiluted samples were placed into a stainless steel vessel (diameter = 34 mm), and strain sweep measurements were taken using a 4-blade vane impeller (diameter = 32 mm, height = 25 mm); viscosity was monitored using the RSI Orchestrator v.6.5.8 program. The angular frequency was 10 rad s^{-1}, and the strain was increased from 1 to 800%.

Solution preparation

Both Zonyl® formulations used incorporate a Foralkyl® perfluorinated monomer, which has a fluorinated carbon number that ranges from 8 to 14 units; the polymers are crystalline in nature. The Zonyls® exist as comb-shaped polymers with fluorocarbon segments. Figure 1 shows the typical structure for both Zonyls®; the aqueous dispersion also contains an alkoxy silane which is not present in the polymer solution. Solutions are made up accounting for the difference in solids content, 25 and 30% by weight for both polymer solution and aqueous dispersion, respectively.

Solvent-borne coating – Zonyl®225

Zonyl®225, an impregnating agent of translucent polymer in butyl acetate (implying that it is a true solution without aggregates), was made up at concentrations of 0.25, 0.5, 1.5, 2.5, 3.5, 4.5, 5.5, and 10.5% solids; this equates to dilution ratios of 1, 2, 10, 14, 18, 22, 30, and 42%, respectively. These were prepared by diluting commercial product in white spirits (Diggers, Australia) and stirring for 1 h.

Aqueous dispersion coating – Zonyl®329

Zonyl®329, a commercially available impregnating agent, is a milky amber-colored aqueous dispersion (polymer colloid). The formulation of this proprietary polymer is such that there are no components added to improve properties. However, trace amounts of solvent (<0.5%) may be present as remnants of the synthesis stage. Samples were made up at concentrations of 0.25, 0.5, 1.5, 2.5, 3.5, 4.5, 5.5, 7.5, and 10.5% solids; this equates to dilution ratios of 0.83, 1.67, 8.34, 11.67, 15.00, 18.30, 25.00, and 35.00%, respectively. These were prepared by diluting the commercial product in Milli-Q water and stirring for 1 h.

Application methods

Application methods were varied to test its effect on the depth of penetration. Coatings were diluted and then applied using two methods: by immersing the terracotta in the diluted coating and by applying the diluted coating with a brush.

Immersion

The terracotta was cut into 57 mm squares, then cleaned twice by soaking in distilled water for 24 h before drying in an oven at 110°C for 48 h. All experiments were conducted at room temperature, ~ 20°C.

After drying, tiles were hung in a 150 mL Zonyl® solution by a piece of cotton thread about 5 cm from the bottom, above a magnetic stirrer running at a low to medium speed. It was important to ensure that the stirring was not too vigorous, to avoid air bubbles forming and clinging to the tile and thus hindering penetration. The tiles were immersed for 15 h, on which they were removed from the solution and hung in a fume-hood to dry for 48 h. All experiments were run in triplicate.

Brush

Terracotta was cut into 200 × 100 mm^2 rectangles and soaked in distilled water twice, each for 24 h. Tiles were then dried in an oven at 110°C for 48 h.

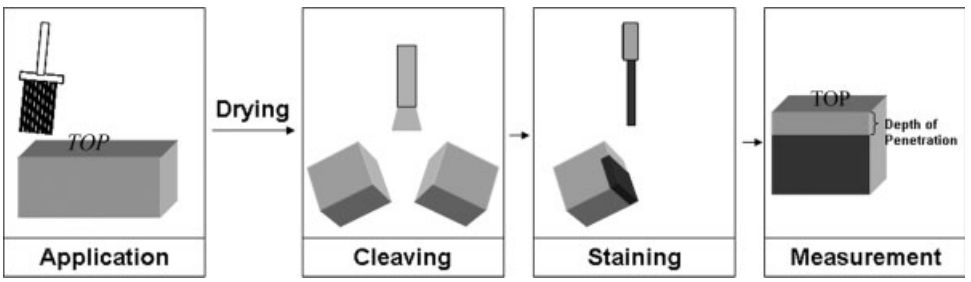

Figure 2 Experimental time-line: coating is applied by multiple applications of a brush on the top; terracotta is then cleaved revealing the cross section; after staining with blue aqueous dye, the depth of penetration of the coating is visible and measurable under low optical magnification.

Solutions were applied onto the top (i.e., smooth surface) of each individual terracotta piece at 400 g m^{-2} (by which is meant applying the amount of coating equivalent to applying 400 g of diluted coating solution to 1 m^2 of tile surface) using an Oldfields Promaster brush with a 50 mm bristle head, at room temperature of $\sim 20^{\circ}C$. A single coat was defined as four brush strokes-two strokes on each half of the terracotta rectangle. The initial stroke showed the greatest deposit of coating; the initial brush stroke was rotated across all four corners to minimize any skewness in the application results. Coatings were applied until the loading amount of 400 g m^{-2} was exhausted. Complete penetration of both coatings into the substrate took between 2 s and 2 min. The brush loaded with coating was weighed after each coat, to ascertain the amount of coating applied per tile. Tiles were then dried for 48 h in a fume-hood. All experiments were run in triplicate.

Cleaving and staining

Figure 2 shows a schematic of the complete experimental process from coating to measuring the depth of penetration. Measurements of penetration depth were made on the cleaved tile. The area of most importance and that for which all data are presented is the top surface; cleaving thus needs to be conducted with minimum impact to the surface. Once coated and dried, tile segments were then cleaved into pieces of roughly 2–3 cm in length, by placing the chisel at the bottom of the terracotta tile and applying pressure with a hammer.

The cross-section was then stained with a blue water-based food coloring by applying one drop at approximately 1 cm intervals to the center of the cross-section (immersion) or to the bottom of the cross-section (brush). This equated to roughly three drops of dye per tile cross-section. Once applied, the dye diffused from the center region, staining the cross-section, and ceasing to spread only in areas where it had contacted the perfluorinated coating. The newly formed boundary was quite distinct, having been created by the water-based dye making contact with the hydrophobic perfluorinated coating; this boundary gives the penetration depth.

Depth of penetration measurement

Once the dye had completely dried ($\sim$ 2 h), measurements of the depth of penetration were made by taking five equidistant measurements from the top surface to the dye front. In this case the top surface is examined, as it is the surface most likely to be exposed and therefore coated with a protective coating when used. It should be noted that there will likely be penetration inhomogeneities on a micron scale, within any one sample; this is purely because of the complexity and heterogeneity of pores across a sample. Despite this, the qualitative difference is insignificant. Although measurements could have been taken across the entire section of terracotta, it was felt that taking all measurements from the same region of the terracotta piece meant that any bias would be constant for the entire set. Measurements were taken using vernier calipers under a magnifying glass, by laying vernier calipers on the surface; the slant of the calipers can then be adjusted to take into account any change in angle on the terracotta section. These values were then plotted as depth (mm) as a function of % solids. Use of a more precise measurement technique such as quantitative light microscopy would not have served any purpose because of the rough nature of the terracotta surface: preparing a profile for light microscopy would require grinding down to a flat surface, which would alter the original profile, rendering such measurements meaningless.

Scanning electron microscopy

Evidence of skin formation were investigated by examining the cross-section using scanning electron microscopy (SEM) with a Phillips XL 30 field emission gun. The SEM had an energy dispersive X-ray spectrometer (EDX) attached for elemental analysis

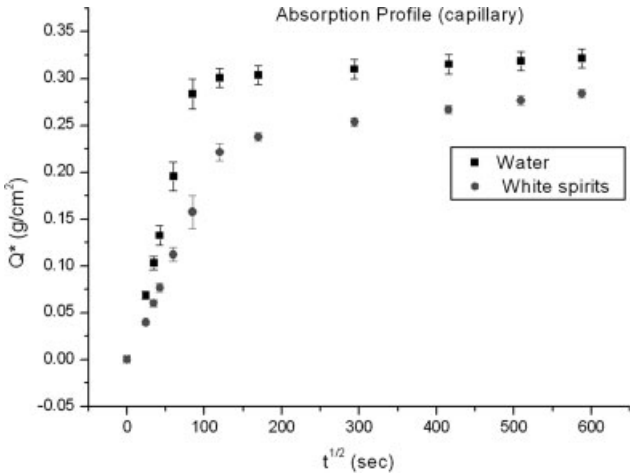

Figure 3 Water and solvent capillary absorption curve for terracotta.

to detect fluorine found in the coating. All specimens were coated with a 20 nm gold coating using an Edwards E306A sputter coater.

RESULTS AND DISCUSSION

Characterization

Absorption by capillarity

Data for the capillary absorption for both white spirits and water as seen in Figure 3 show a marked difference in absorption coefficients. For water, $A = 0.0032$ g cm^{-2} s$^{-1/2}$ compared with that of white spirits, where $A = 0.0018$ g cm^{-2} s$^{-1/2}$. Such a difference in penetration rates can be ascribed to the hydrophilic nature of the terracotta: unlike water, a nonpolar solvent such as white spirits will have little interaction with the pore surface.

Absorption by immersion

This method is typically used to test the efficacy of pretreated samples; in this case, however, it was used to look at the uptake of both solvent/dispersant as well as the polymer solution/dispersion at concentrations used in the brush and immersion process.

The steep leading edge of the absorption curves is a familiar feature which is used to determine the absorption coefficient. This is associated with a diffusivity function which increases rapidly with water content.[26] With increased density and viscosity, as is the case with higher concentrations, there is a decrease in the maximum absorption by weight fraction (Q_{imm}) of impregnating agent. This is visible in the absorption curve by immersion in the water-based dispersion (Fig. 4). There is, however, no visible increase or trend when this was conducted in solution. Although the rates of absorption have little variation between both polymers, the maximum (Q_{imm}) is different for the aqueous- and solvent-based polymers, with the aqueous dispersion showing a higher rate of absorption. Accompanying this, we see small anomalies between differing concentrations of the same coating: the aqueous dispersion at 0.5% concentration shows a higher Q_{imm} value than that of water. Although we have no definitive explanation for this behavior, present only over a small range, we speculate that it arises from complex surface interactions between the various water-soluble species present; its presence is immaterial for the purposes of explaining the differences in absorption rates.

Absorption data for the polymer solution do not show a typical plateau, instead taking up to 120 h to reach the saturation achieved by the water-based dispersion. The aqueous dispersion achieves total saturation within the first 10 h; this is not the case with the solvent-based polymer. This difference is ascribed to an effect of the solvent polarity, as discussed in connection with data from absorption by capillarity.

Viscosity and molecular weight

A large difference in molecular weights was found between both dispersion and solution. This will affect the ability of the polymer to coat both the surface and the pores on evaporation of the dispersant/solvent, but will not play a great role in determining the depth of penetration in immersion measurements, other than the effect the value has on viscosity.

Viscosity will usually be a function of the molecular weight. The polymer dispersion showed a range of between 6×10^5 and 1×10^6 g mol^{-1} compared

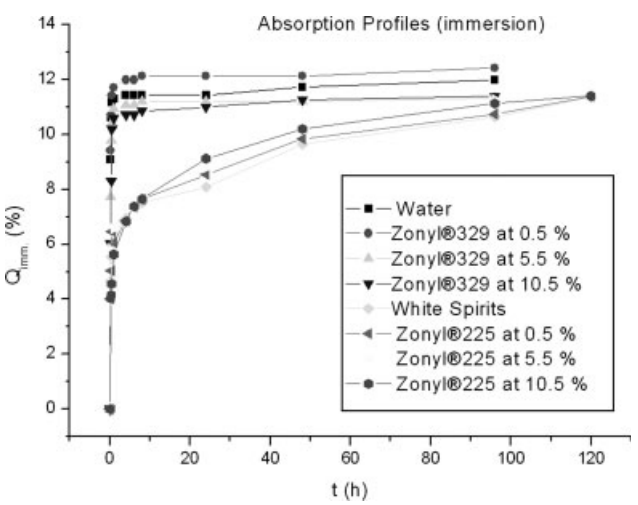

Figure 4 Water/solvent/polymer absorption curves for terracotta by immersion at varied concentrations.

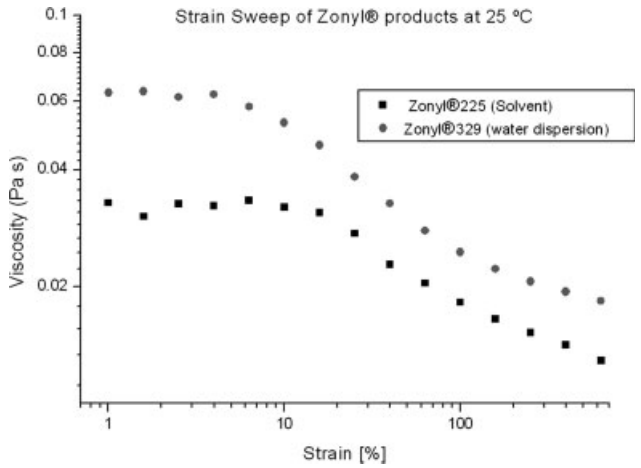

Figure 5 Strain sweep behavior of both Zonyl® products.

with the polymer solution which had a range of 2×10^4 to 5×10^4 g mol^{-1}. Regardless of the large molecular weight differences, it was found that both viscosities for the undiluted system were quite low (Fig. 5). Thus, it is expected that viscosity effects in this system will play an unimportant role. Both polymers exhibited shear thinning behavior.

Zeta potential for pores and particles, pH, conductivity, and particle size

The pH of the terracotta pores as determined with EKA (Fig. 6) showed a slightly negative surface charge, ranging between −2.4 and −1.6 mV for Milli-Q water at pH of 4.6–4.7, that is, within the range of that used in the brush and immersion process for the water dispersion. The surface charge of the polymer dispersion as a function of concentration shown in Figure 7 showed a positive zeta potential that was between 60 and 70 mV. With a negative pore surface and positive charge on the

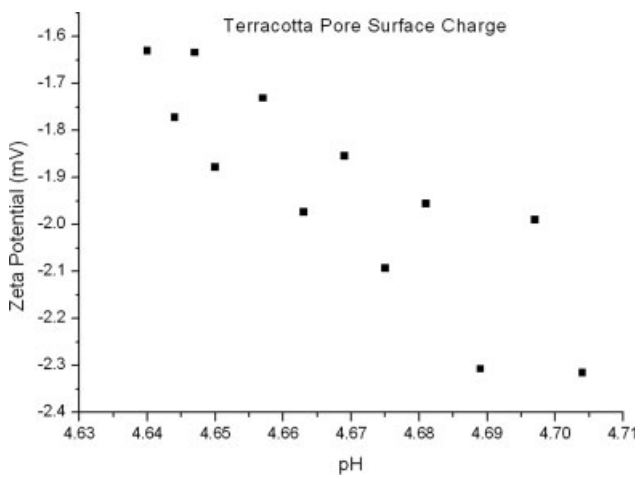

Figure 6 Pore surface charge of terracotta at acidic pH as used in the coating process.

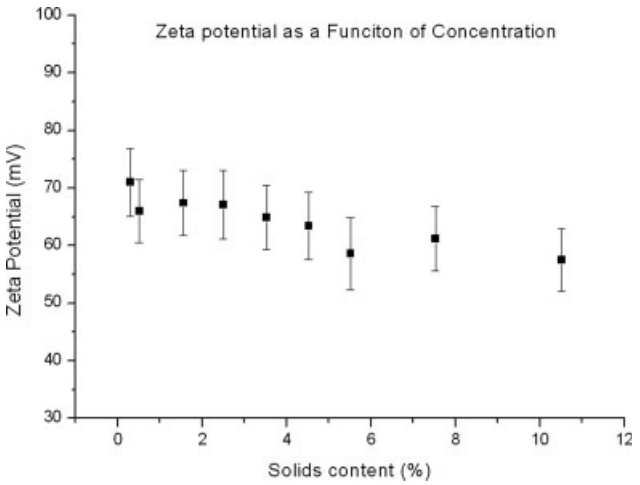

Figure 7 Surface charge of the cationic Zonyl®329 as a function of concentration.

particle surface, electrostatic forces are likely to play an important role in affecting penetration depth.

The pH of solutions used in the coating process showed little variation with concentration (Fig. 8), with no concentration showing a pH outside the range 4–5; therefore, one could not expect there to be a great difference in zeta potential for particles across the different concentrations. Conductivity measurements showed an increase with concentration (Fig. 9) up to a maximum of 2 mS cm^{-1} at 10.5% solids. Particle size measurements (Fig. 10) showed the presence of two populations, the smaller at $\sim$ 0.07 μm and the larger at $\sim$ 0.4 μm.

The radius of gyration of the polymer coils in the organic solution (Zonyl® 225) was not measured, but can be estimated from standard models for chain dimensions and typical values for characteristic ratios to be $\sim$ 102 nm, orders of magnitude smaller than pore sizes.

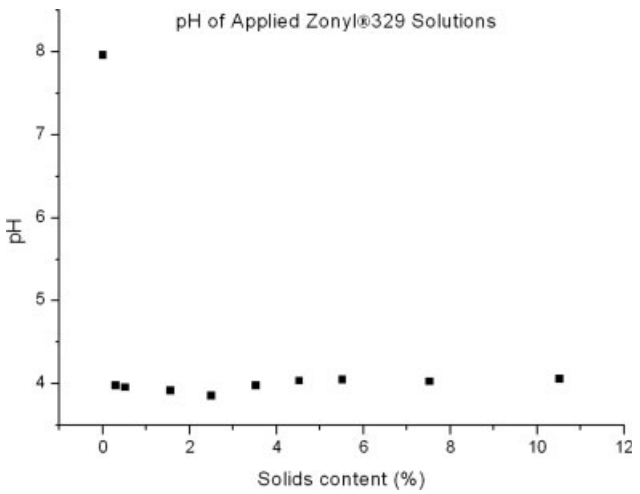

Figure 8 pH of water-based dispersion with varying solids content.

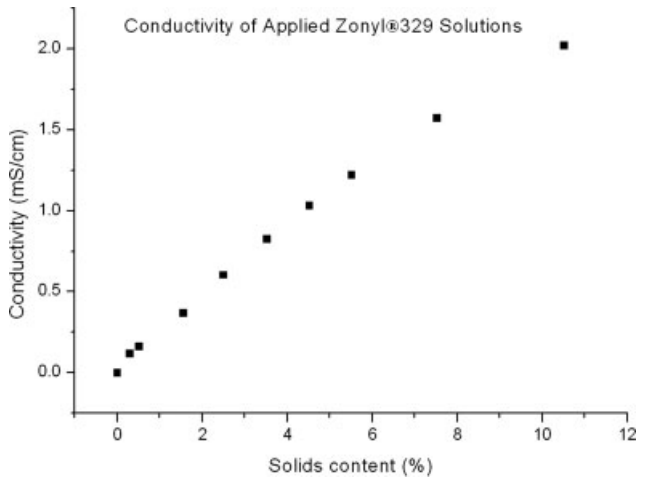

Figure 9 Conductivity of water borne dispersion as a function of concentration.

Porosimetry

Mercury porosimetry data shown in Table I show a median pore diameter (area) of 0.109 μm and a porosity of 33.2%. This is an important detail when dealing with the penetration of colloids as in the water based dispersion, as this sets the maximum penetration physically possible for a colloid population of a given particle size. The pore-size distribution yielded by mercury porosimetry is shown in Figure 11, and shows that the porosity is bi-modal, with the majority of pores being below 0.44 μm (as measured down to a limit 0.006 μm).

Thermal properties

DSC data (Table II) showed the presence of two glass transition temperatures (T_g) on the second heating for the solvent-based impregnating agent,

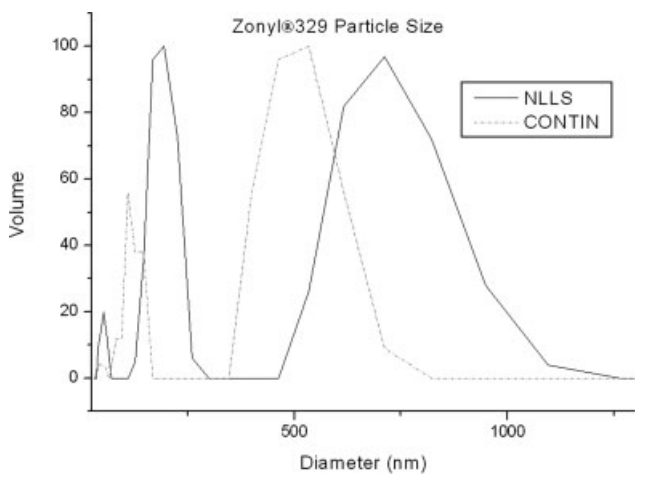

Figure 10 Volume particle size distribution of water dispersion obtained by deconvoluting data from using dynamic light scattering (DLS).

TABLE I
Mercury Porosimetry Analysis

Median pore diameter (area) (μm)	0.109
Media pore diameter (volume) (μm)	0.3741
Bulk density (g cm^{-3})	1.978
Apparent (skeletal) density (g cm^{-3})	2.962
Porosity (%)	33.2

Gauge pressure = 4.8 × 103 Pa.

whereas only a single T_g was evident in the case of the water-based dispersion. The isotropization temperature (T_i) was found to be 52°C for the polymer solution and was not measureable for the dispersion. On cooling, crystallization exotherms (T_c) were found at 46°C for the polymer solution and 47°C for the polymer dispersion. As discussed later, crystallization probably only affects the penetration depth with respects to the brush application and will not have any influence on the immersion depth of penetration.

Surface tension

The surface tension as a function of concentration plotted in Figure 12 shows a surface activity for the dispersion that was almost double that in the polymer solution. Surface activity of the impregnating agent is likely to affect the wetting ability and hence the depth of penetration. This can be seen through a simplified capillary pressure equation for noncylindrical pores:[27]

$$P_c = \frac{2(\sigma_{sg} - \sigma_{s1})}{r} \quad (4)$$

Here P_c is the capillary pressure, σ_{sg} the surface energy at the solid–gas interface, σ_{sl} the surface

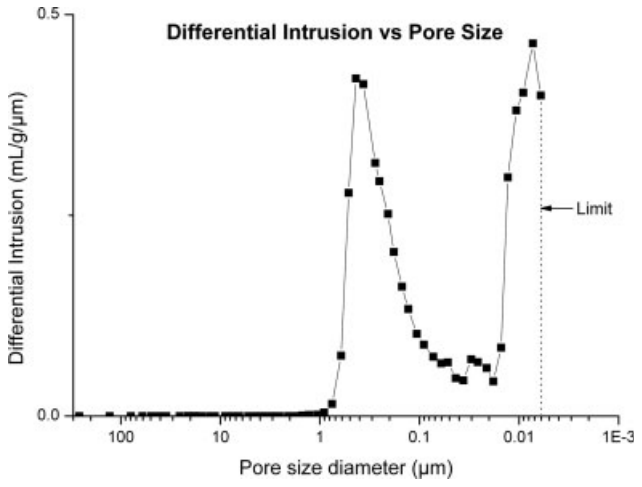

Figure 11 Mercury porosimetry data, showing a bi-modal terracotta pore size distribution.

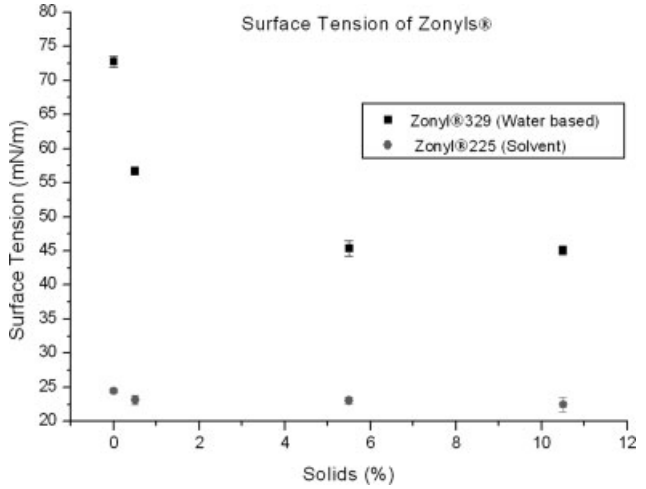

Figure 12 Surface tension trends for both polymers.

energy at the solid–liquid interface, and r the radius of the pore.

From the results shown in Figure 12 it is expected that the higher surface tension found with the aqueous dispersion suggests poor wetting ability in comparison with the solvent-based polymer because of the lower adhesion forces.

X-ray diffraction

X-ray diffraction of two sections was conducted (Fig. 13) in order see if there was any significant chemical difference between the exposed surface layer and the bulk terracotta. The terracotta was found to consist primarily of quartz, anorthite (calcium aluminosilicate), and kaolinite. There was no difference between both diffraction plots, and thus we assume little change with surface polymer interaction as the polymer front proceeds forward.

Depth of penetration (immersion)

Figure 14 shows a typical image of a cleaved and stained cross section from the immersion method. Penetration measurements are taken from the top surface of the section, as this is the region that will be exposed in an outdoor setting and therefore needs protection. In immersion, penetration occurs from all possible sides; this explains the unstained regions to the side and bottom of the image: since Figure 14 shows a section of the complete cleaved tile, the penetration depth around the perimeter is not continuous.

Figure 15 shows penetration depth as a function of concentration of polymer for both Zonyls® with application by immersion. Not unexpectedly, both coatings show increasing penetration with increasing concentration; this is governed and can be explained by simple diffusion. At the lowest concentration of 0.5% solids, both coatings show the same penetration depth. This effect occurs well below the recommended application level of the products, and is therefore not significant. A possible expalanation is that the pore network of the terracotta could begin to change at such a depth below the surface (which is exposed during the manufacturing process), although this is purely speculation.

The slopes of penetration depth against concentration of these plots show that the polymer solution has a slope that is 2.6 times steeper than that of the aqueous dispersion. This is at first surprising, considering the absorption by immersion data in Figure 4 shows a higher rate of absorption by the aqueous system. Such a high penetration of the polymer solution compared with the aqueous dispersion could be because of any or all of the solubility of the polymer

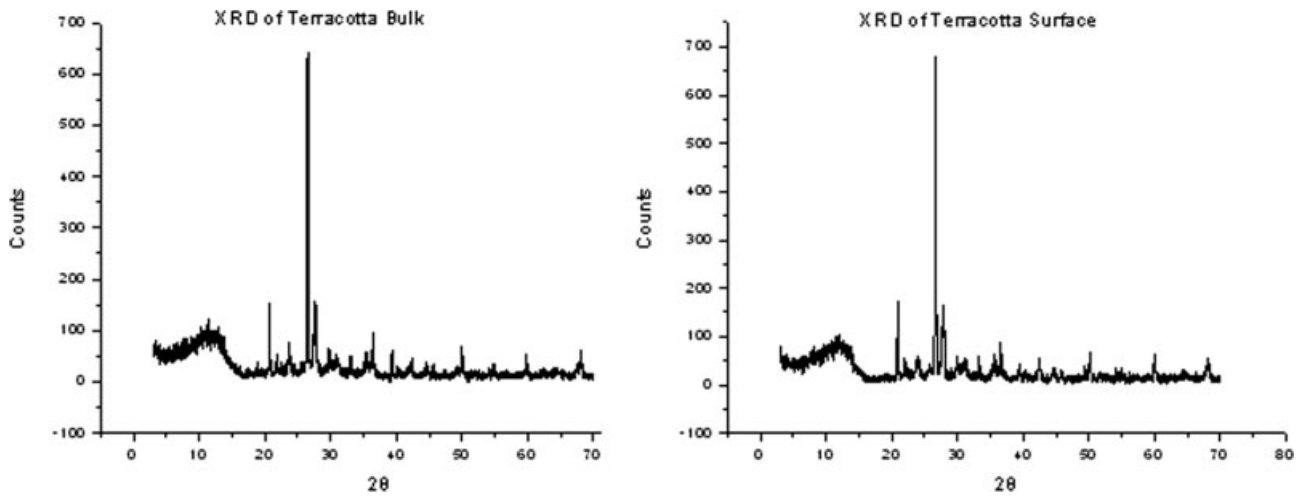

Figure 13 XRD from the surface and bulk.

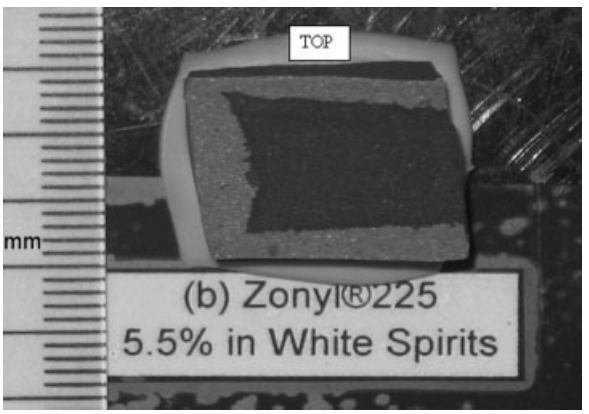

Figure 14 A cross section of terracotta immersed in the polymer solution and stained with blue dye (center), penetration measurements are taken from the surface (top).

in solution and interactions between polymer and substrate. Such observations can be rationalized in terms of other factors that are likely to affect the polymer dispersion, as discussed later.

The lower depth of penetration as seen with the polymer dispersion compared with the polymer solution presumably arises from more than one effect. One of these is probably the adsorption of the positively charged particles as determined by zeta potential measurements (Fig. 7) onto the negatively charged surface both within the pores and on the surface (Fig. 6). This will restrict pore size and therefore restrict penetration. However, in the immersion measurement, penetration continues to take place as smaller particles work their way past adsorbed particles deeper into the pore network.

The polymer solution is completely soluble in the nonpolar white spirits as opposed to the aqueous dispersion, where the polymer chains are in discrete particles. Such differences means that porosity of the terracotta will not affect the depth of penetration of the polymer solution as strongly as it would the aqueous dispersion; hence we see a difference in overall penetration depths yet similar trends. Such trends are probably because of the more mobile smaller population of particle sizes <0.1 μm (Fig. 10) having more time in the immersion experiment to penetrate deep into the network. The larger population of $\sim$ 0.4 μm will experience porosity-limited penetration, as the terracotta has a median porosity of 0.109 μm (Table I).

The differences in surface activity between both polymers could also have a dramatic effect on the penetration depth as seen with the immersion procedure. Given that both the solid–gas surface energy (σ_{sg}) and the radius remain constant for both applications, then from eq. (4), the only difference between the effects of each polymer will be the surface energy at the solid–liquid interface (σ_{sl}). Despite the higher surface tension of the aqueous dispersion,

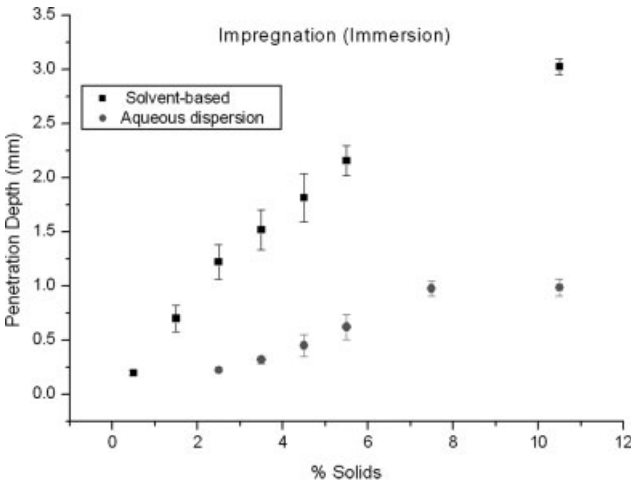

Figure 15 Depth of penetration as a function of concentration for coating by immersion, for both polymer solution and aqueous dispersion.

it can be speculated that the aqueous dispersion will have a greater affinity for the surface, as seen in Figure 4, where the aqueous dispersion shows a much higher weight fraction percent (Q_{imm}) value for the dispersion than the solution. This is due to the hydrophilic nature of the material. Thus it will spread more easily, giving a lower surface energy at the solid-liquid interface (σ_{sl}). This gives a higher capillary pressure (P_c) and thus greater penetration properties. Unlike the brush application case discussed later, with the immersion there will be little change with surface tension, as the polymers do not undergo any evaporation or loss of medium.

Depth of penetration (brush)

Figure 16 shows the depth of penetration plotted against the concentration for the solvent-based system

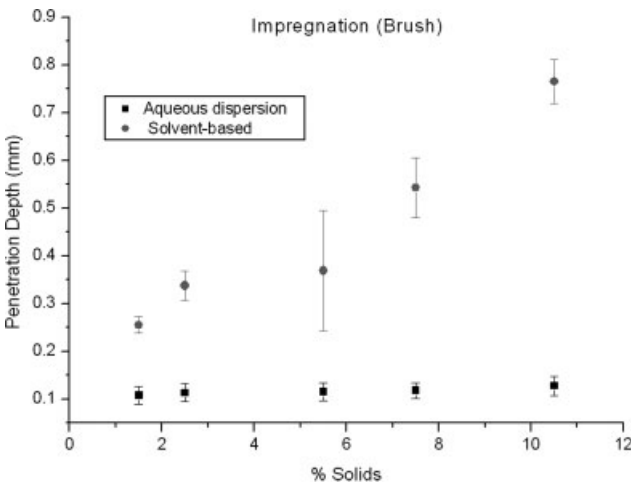

Figure 16 Depth of penetration as a function of concentration for coating by brush, for both polymer solution and aqueous dispersion

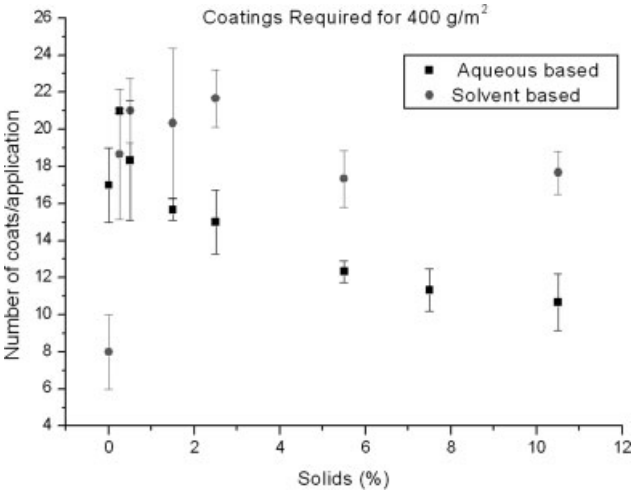

Figure 17 Number of applied coatings required for 400 g m^{-2}.

when applied by brush. Again, it is expected that higher polymer concentration in the coating would lead to higher penetration depth. While Figure 16 shows the polymer solution exhibiting the expected trend, the aqueous dispersion displays a featureless depth of penetration across all concentrations.

From the capillary absorption data in Figure 3, one would expect the terracotta pore network to favor a higher penetration depth for the aqueous dispersion. By comparing absorption coefficients of the aqueous dispersion, $Q_{cap} = 0.0032$ g cm^{-2} $s^{-[1/2]}$, which is almost double that of the polymer solution, where $Q_{cap} = 0.0018$ g cm^{-2} $s^{-1/2}$, it would at first be expected that the terracotta should have more polymer imbedded within the network. This, however, is the opposite of what is seen in Figure 16. The next step is to look at the viscosity differences between both polymer mixtures as applied to the surfaces (Fig. 5), since significant viscosity differences would obviously affect penetration. However, the applied polymer mixtures have low viscosities, approaching those of the pure continuous phase/solvent, and there is little difference between these. This suggests that adsorption effects of the cationic aqueous dispersion onto the negatively charged terracotta pore surface, as seen in Figure 6, might explain the observation that the water dispersion has the lower penetration depth.

The existence of a negative charge on the terracotta surface, as seen in Figure 6, compared with the positively charged colloids in the dispersion in Figure 7, suggests that particles are likely to stick to any free surface found within the pores as a result of the attractive charges. The presence of such particles within the pores reduces the median pore diameter below the average of 0.109 μm (Table I), making further penetration by the dispersion unlikely.

The brush application differed slightly in the amount of brush strokes required to obtain the correct loading of impregnating agent onto the terracotta, as seen in Figure 17. Here the polymer solution required more brush strokes to obtain the same loading. Although this would play a marked effect on the penetration depth as the downward pressure of the brush strokes force solution further into the pore network, it is also a function of the polymer viscosity (Fig. 5) and the holding ability of the bristles to both polymers.

This unexpected lack of dependence of depth on applied concentration with brush application can be interpreted to arise from a series of phenomena working collectively to prevent any further penetration beyond ~ 0.12 mm. With both coatings, individual side chains at the surface/air interface can arrange themselves upon drying in various ways depending on the length of the side chain ($—C_nF_{2n+1}$),[28] the length and nature of the spacer or the main chain flexibility.[29] These crystalline segments comprising the fluoroalkyl side chains are what give perfluorinated polymers such low surface tensions relative to amorphous polymers.[30] Similar crystallization temperatures, as recorded by DSC in Table II for both polymer solution and aqueous dispersion of 46°C and 47°C, respectively, suggest the common perfluorinated chains shared by both are likely to undergo partial crystallization between brush strokes, as applications were conducted with drying of the previous coating. In this case, the fluoroalkyl groups would be oriented to the outermost layer of the polymer/air interface, which makes it likely that any subsequent application of coating will lead to the deposition of polymer on top of the previous layer with little to no diffusion of polymer.

The existence of such a layer at the surface does not allow for future retreatment if the need arose. Typically a surface impregnated with Zonyl® is retreated by adding specially designed fluorinated surfactants at small concentrations to the coating; this lowers the surface tension of the solution, thereby increasing the wetting properties and thus allowing the coating to penetrate the hydrophobic/oleophobic surface. Such retreatment is not possible with such a polymer-clogged surface. The data in Figure 12 show a surface tension approximately twice as high for the aqueous dispersion as that for the polymer solution; therefore the wetting properties of the polymer solution should be greater in comparison with the aqueous dispersion.

TABLE II
Thermal Analysis for Both Zonyls®

	T_g (°C)	T_i (°C)	T_c (°C)
Zonyl®225	−9 37	52	46
Zonyl®329	47	–	47

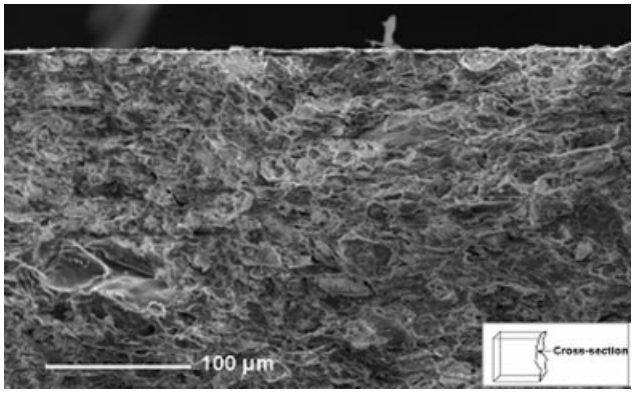

Figure 18 Cross-section of untreated terracotta obtained using SEM; arrow in insert here and in later figures indicates the direction in which the micrograph is taken.

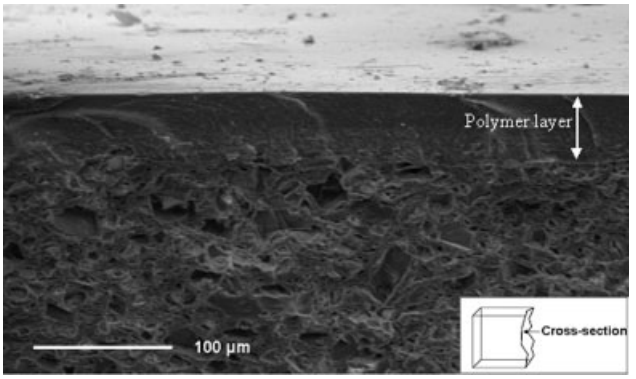

Figure 19 Cross-sectional view of terracotta brush-coated with the aqueous dispersion at 240 gm^{-2} showing a layer (smooth region) formation on the surface.

SEM microscopy was employed to garner evidence for or against this postulate. Figure 18 shows a typical SEM image of a cross section of untreated terracotta. Figure 19 shows a SEM micrograph of the cross section brush-coated with 240 g m^{-2} of the aqueous-dispersion coating. This shows a layer (smooth region) formation on the surface, supporting the postulate of a polymer layer forming on the surface of the terracotta. The presence of this polymer layer in this brush-coated substrate probably occurs because the fluoroalkyl-chains prevent any water from penetrating into the pores, thus preventing penetration of the polymer; this is termed autorepellency and leads to skin formation in perfluorinated acrylates.

Figure 20 shows an SEM image of a cross-section of terracotta brush-coated with the polymer solution; here there seems to be very little difference compared with the untreated cross-section of Figure 18. Although crystallization will take place in both coatings, it has no effect on the polymer solution, as its good solubility in white spirits suggests that any application of another coat will only redissolve the crystallized segments. This allows for penetration to continue unhindered, explaining why we do not see any evidence of skin formation when looking at the solvent-based coated cross section of Figure 20. The resulting lack of auto-repellency explains the rise in polymer penetration with increasing concentration for the polymer solution observed in Figure 16.

Autorepellency will only affect application methods which allow for polymer/air interface to form on the substrate; this includes brush. Autorepellency should not affect techniques that require a single application, such as flow coating.

Another possible explanation for the independence of concentration for the dispersion is as follows. The smooth polymer layer as seen on the top of the cross-section SEM micrograph in Figure 19 for the water-based dispersion might be explained by surface pore blockage that commences with particles being both chemically and electrostatically bound to the substrate. The presence of an alkoxy silane in the water dispersion formulation and its absence from solvent-based coating leads us to believe that additional interactions involving the alkoxy silane and silicon in the terracotta could lead to pore blockage and therefore restrict penetration. Alkoxy silanes are added into the formulation the water dispersion to improve the polymer/substrate compatibility based on the hydrolysis and condensation reactions with silanol groups found on the substrate.[11] These alkoxy silanes have also been used as consolidants for atmospherically corroded stone, incorporating the same hydrolysis/condensation reactions.[30]

The hydrolysis reaction of the alkoxy silane, which is catalyzed in acidic conditions, allows the hydrolyzed group to undergo a condensation reaction

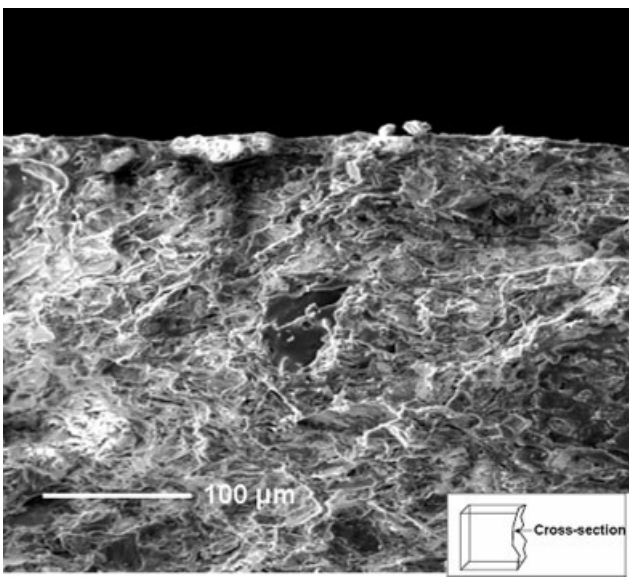

Figure 20 Cross-sectional view of terracotta brush-coated with 240 g m^{-2} of the polymer solution; here there is no evidence of a layer formation.

with other silanol groups found in both polymer and substrate. The reactions are as follows:[29]

$$\text{Hydrolysis: } A\text{SiA}(\text{OAR}_2)_3 + 3\text{H}_2\text{O} \rightarrow \text{ASiA}(\text{OH})_3 + 3\text{HOR}_2(\text{R}_2 = \text{alkyl group}) \quad (5)$$

$$\text{Condensation: } A\text{Si}(\text{OH})_3 + \text{ASi}(\text{OH})_3 \rightarrow \text{ASi}(\text{OH})_2\text{AOASi}(\text{OH})_2 + \text{H}_2\text{O} \quad (6)$$

It should be noted that alkoxy silane condensation reactions are pH sensitive, and that the condensation reaction is the rate-limiting step for silanes at the acidic pH used, that is, pH between 4 and 5; this is well known within the sol-gel method, and is applicable in this case to the current system.[31–35] In Zonyl®329 a monoacid is added to stabilize the alkoxy silane and function as condensation inhibitor.[36] Therefore, when Zonyl®329 is applied, the silane reaction will not act immediately; however, the condensation rate should increase as the water is removed, whether through evaporation or further penetration [eq. (5)]. The only foreseeable influence the presence of an alkoxy silane will have on the rate of penetration would be by modifying the polarity of the polymer. Therefore, its presence in only the water dispersion and absence from the solvent based Zonyl®225 makes little immediate difference to the penetration depth.

These reactions might lead to pore blockage and eventually skin formation if the colloids are bound to the surface by both processes, and are sufficiently large to block the pores. While no such effect was observed with immersion coating of the water-based dispersion, it is conceivable that the above reactions might take place only with the changes in ionic strength and pH occurring as the coating dries between applications. The ionic strength of the aqueous dispersion increases with increasing concentration as observed the conductivity measurements in Figure 9, but there is only a slight effect on the surface charge of the particle (Fig. 7).

Pore blockage was assessed by looking at the particle sizes for water dispersion and correlating this to median pore size of substrate (Table I). Being in solution with no aggregates means the solvent-based coating is exempt from such interaction. Particle size distribution measurements were conducted using dynamic light scattering (DLS) and data were fitted using the CONTIN method,[15] the results of which are shown in Figure 10. It is essential to be aware that DLS, because it does not physically separate by size, cannot give an unambiguous particle size distribution, and instead the time-dependent scattering intensity comprising the raw DLS data is inverted to a size distribution making various assumptions. This inversion is a mathematically ill-conditioned problem: a correct answer can only be obtained with infinitely precise data over an infinite range, and the inversion procedure is prone to numerical artifacts. Any features in a size distribution produced by DLS software must be tested for artifacts by varying the basic assumptions as to the form of the distribution (e.g., CONTIN versus NLLS[37,38]) and numerical parameters in the inversion such as integration range. The bimodal distribution in the size distribution found in the water dispersion remained stable over different integration ranges for both CONTIN and NLLS, suggesting the bimodality was not a DLS artifact.

The data in Figure 10 show two populations, with the largest being $\sim$ 0.4 μm. This suggests that pores less than 0.4 μm will filter the majority of the particles, acting as a sieve for the larger colloids. Considering the median (area-average) pore size is approximately five times less than this population at 0.109 μm (Table I), it is easy to see how this can be a limiting factor to maximum depth of penetration. Figure 21 shows an SEM micrograph of an untreated surface, like that shown in Figure 22 shows a magnified pore on the same surface. The presence of smaller pores is immediately evident on magnification of the larger surface pores, which can also be seen on the surface of the terracotta. It is within these pores that the polymer sieving is expected to take place, ultimately blocking the larger surface pores, which are on average $\sim$ 20 μm in diameter. It should be noted here that although pores less than 0.4 μm will block the majority of particles, all smaller pores shown will reduce the impregnation depth of polymer, by restricting free flow. Since this does not occur for immersion application of the water-based dispersion, any such effect must be induced by the changes in ionic strength and/or pH during drying.

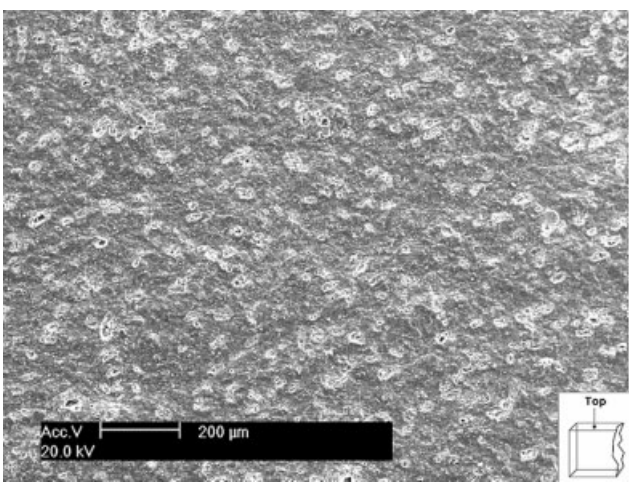

Figure 21 SEM image showing porous untreated terracotta surface; pores seen as white circular regions due to charging of the surface under electron microscope.

Figure 23 shows the results of EDX spectroscopy within 50 μm from the surface for untreated and treated cross-sections. Untreated terracotta shows of course a high concentration of silicon present as quartz, as seen in the X-ray diffraction pattern in Figure 13. Whereas the treated surfaces show the presence of fluorine imparted by the polymer. The detection of fluorine is greatly enhanced in the aqueous dispersion because of the higher concentration on the surface and thus lower penetration depth. This is not as visible in the polymer solution arising from the higher penetration depth, and thus smaller concentration on the surface. Interestingly, there is little to no compositional difference as one moves down through the terracotta cross-section as seen in Figure 13. This will limit any chemical interactions with polymer because of mineralogical differences.

The fact that the solvent system is still good at surface protection, despite the greater penetration depth, and hence lower local concentration, shows that very little fluorine is required to impart hydrophobic properties to a surface.

CONCLUSIONS

In this work, we have shown the influence of the application method on the depth of penetration for two perfluorinated acrylates: an aqueous-based dispersion of colloid particles (Zonyl®329) and a polymer solution (Zonyl®225). The two methods of applying the coating were chosen to select the two major groups of coating applications: immersion (a single-application technique) and brush (a multiapplication technique). It was found that using immersion increases the depth of penetration into a porous substrate such as terracotta, and that penetration depth differs depending on the formulation of the coating. Data for the solvent-borne system show that good surface protection can be obtained with low polymer concentrations in the substrate.

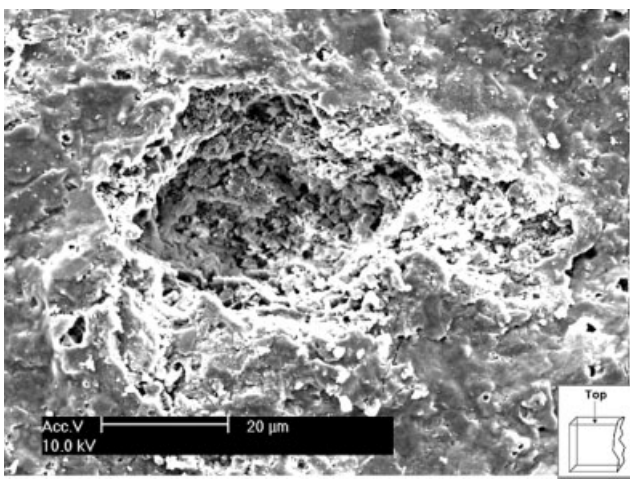

Figure 22 SEM image of a pore, average sized pore ranges between 20 and 40 μm.

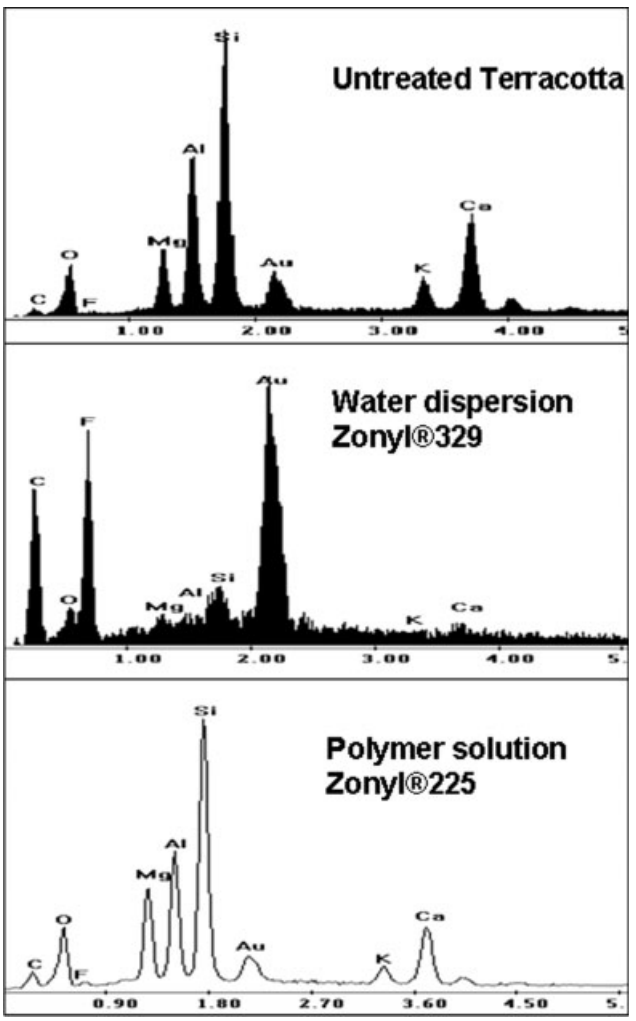

Figure 23 EDX spectra of untreated and treated cross sections between 0 and 50 μm from the surface.

It was found that the aqueous dispersion forms a skin when applied by brush. Such a skin prevented any penetration beyond ~ 0.12 mm in the system studied here. This effect may be amplified by covalent bonding of the polymer to the silicon in terracotta during the drying process between applications, but also seems to be limited by the limited pore size of the terracotta which restricts the larger sized particle population. Such pore restrictions seem to be exacerbated by electrostatic attraction, as seen with the positively charged particles coming adsorbing onto the negatively charged terracotta at pH between 4 and 5. The solvent-based Zonyl®225 did not show any such formation, with the trends in penetration depth remaining the same across both techniques.

Such work, looking at the coating behavior of different formulations of fluorinated acrylates, will allow us to elucidate the mechanisms involved

between porous substrates and coatings that have been designed to impart both hydrophobic and oleophobic properties. This will lead to better synthesis design to suit not only surface properties of substrate based on porosity and chemical composition but also the ability to design fluorinated coatings with high depth of penetration in mind that will suit a wide range of application methods ranging from immersion to spray techniques.

References

1. Keller, W. D. Principles of Chem Weathering; Lucas Brothers Publishers: Columbia, MO, 1957.
2. Warscheid, T.; Braams, J. Int Biodeterior Biodegrad 2001, 46, 343.
3. Searle, D. E.; Mitchell, D. J. Land Reconstr Manage Ser 2004, 3, 1.
4. Kucukkaya, A. G. NATO Sci Ser Ser 2: Environ Security 1999, 57, 215.
5. Massey, S. W. Sci Total Environ 1999, 227, 109.
6. Lorusso, S.; Marabelli, M.; Troili, M. J Environ Pathol Toxicol Oncol 1997, 16, 171.
7. Kucera, V.; Fitz, S. Water Air Soil Pollution 1995, 85, 153.
8. Davini, P. Inform Marmista 2005, 44, 45.
9. Winkler, E. M. Stone: Properties, Durability in Man's Environment; Springer: New York, 1975.
10. Lopez-Acevedo, V.; Viedma, C.; Gonzalez, V.; La Iglesia, A. J Crystal Growth 1997, 182, 103.
11. Pabon, M.; Perdon, A.; Peeters, H.; Pitture e Vernici. Eur Coat 2006, 82, 58.
12. Feiring, A. E.; Wonchoba, E. R. Macromolecules 1998, 31, 7103.
13. Hayes, L. J. J Fluorine Chem 1976, 8, 69.
14. Dubois, M.; Guerin, K.; Giraudet, J.; Pilichowski, J. F; Thomas, P.; Delbe, K.; Mansot, J. L.; Hamwi, A. Polymer 2005, 46, 6736.
15. Ciardelli, F.; Aglietto, M.; di Mirabello, L. M.; Passaglia, E.; Gianscristoforo, S.; Castelvetro, V.; Ruggeri, G. Prog Organic Coatings 1997, 32, 43.
16. Anton, D. Adv Mater (Weinheim, Germany) 1998, 10, 1197.
17. Antonucci, V.; Mastrangeli, C.; Mensitieri, G.; Del Nobile, M. A.; Nicolais, L. Mater Structur 1998, 31, 104.
18. Dreher, W. R.; Jarrett, W. L.; Urban, M. W. Macromolecules 2005, 38, 2205.
19. Castelvetro, V.; Ciardelli, F.; Francini, G.; Baglioni, P. Macromol Mater Eng 2000, 278, 6.
20. Castelvetro, V.; Aglietto, M.; Ciardelli, F.; Chiantore, O.; Lazzari, M.; Toniolo, L. J Coat Technol 2002, 74, 57.
21. Poli, T.; Toniolo, L.; Chiantore, O. Appl Phys A: Mater Sci Process A 2004, 79, 347.
22. Van, T. T.; Beck, K.; Al-Mukhtar, M. Environ Geol (Heidelberg, Germany) 2007, 52, 283.
23. Normal Protocol 11/85. Water Absorption by Capillarity—Capillarity Absorption Coefficient; ICR-CNR: Rome, 1986.
24. Normal Protocol 7/81. Water Absorption by Complete Immersion—Capacity of Imbibition; ICR-CNR: Rome, 1981.
25. Kuang, C. S.; Yee, W. Y.; Shaari, S. Sci Technol Adv Mater 2005, 6, 383.
26. Carpenter, T. A.; Davies, E. S.; Hall, C.; Hall, L. D.; Hoff, W. D.; Wilson, M. A. Mater Struct 1993, 26, 286.
27. Larson, B. US Department of Transportation (DOT/FAA/AR-01/95), Washington DC, 2002.
28. Imrie, C. T.; Karasz, F. E.; Attard, G. S. Macromolecules 1992, 25, 1278.
29. Volkov, V. V.; Plate, N. A.; Takahara, A.; Kajiyama, T.; Amaya, N.; Murata, Y. Polymer 1992, 33, 1316.
30. Kotlik, P. Chem Listy 1987, 81, 511.
31. Tan, B.; Rankin, S. E. J Phys Chem B 2006, 110, 22353.
32. Rankin, S. E.; McCormick, A. V. Chem Eng Sci 2000, 55, 1955.
33. Kay, B. D.; Assink, R. A. Mater Res Soc Symp Proc 1986, 73, 157.
34. Sefcik, J.; McCormick, A. V. Catal Today 1997, 35, 205.
35. Assink, R. A.; Kay, B. D. J Non-Crystalline Solids 1988, 99, 359.
36. Sanchez, J.; McCormick, A. J Phys Chem 1992, 96, 8973.
37. Cao, X.; Sessa, D. J.; Wolf, W. J.; Willett, J. L. Macromolecules 2000, 33, 3314.
38. Bello-Perez, L. A.; Roger, P.; Colonna, P.; Paredes-Lopez, O. Carbohydr Polym 1998, 37, 383.